The O_2 Binding Pocket of Myohemerythrin: Role of a Conserved Leucine†

Junjie Xiong,‡ Robert S. Phillips,‡ Donald M. Kurtz, Jr.,*,‡ Shi Jin,‡ Jingyuan Ai,§ and Joann Sanders-Loehr§

Department of Chemistry and Center for Metalloenzyme Studies, University of Georgia, Athens, Georgia 30602-2556, and Oregon Graduate Institute of Science & Technology, P.O. Box 91000, Portland, Oregon 97291-1000

Received December 23, 1999; Revised Manuscript Received April 24, 2000

ABSTRACT: A conserved O_2 binding pocket residue in *Phascolopsis gouldii* myohemerythrin (myoHr), namely, L104, was mutated to several other residues, and the effects on O_2 association and dissociation rates, O_2 affinity, and autoxidation were examined. The L104V, -F, and -Y myoHrs formed stable O_2 adducts whose UV−vis and resonance Raman spectra closely matched those of wild-type oxymyoHr. The L104V mutation produced only minimal effects on either O_2 association or dissociation, whereas the L104F and -Y mutations resulted in 100−300-fold decreases in both O_2 association and dissociation rates. These decreases are attributed to introduction of steric restrictions into the O_2 binding pocket, which are not present in either wild-type or L104V myoHrs. The failure to observe increased O_2 association or dissociation rates for L104V indicates that the side chain of leucine at position 104 does not sterically "gate" O_2 entry into or exit from the binding pocket in the rate-determining step(s). L104V myoHr autoxidized approximately 3 times faster than did wild type, whereas L104T autoxidized $>10^6$ times faster than did wild type. The latter large increase is attributed to increased side chain polarity, thereby increasing water occupancy in the oxymyoHr binding pocket. These results indicate that L104 contributes a hydrophobic barrier that restricts water entry into the oxymyoHr binding pocket. Thus, a leucine at position 104 in myoHr appears to have the optimal combination of size and hydrophobicity to facilitate O_2 binding while simultaneously inhibiting autoxidation.

Hemerythrin (Hr) and myohemerythrin (myoHr) are nonheme iron, O_2-carrying proteins found in coelomic cells and muscle tissues, respectively, of a few marine invertebrate phyla. MyoHr is monomeric, but otherwise closely resembles the oligomeric Hr in both structure and function. Characteristic features defining the Hr/myoHr subunit include a four-helix bundle protein backbone surrounding an oxo-/hydroxo-bridged diiron site, the structure of which is shown schematically in Scheme 1 (*1*). A distinctive amino acid sequence motif, shown in Figure 1, furnishes five terminal histidine and two bridging carboxylate ligands to the diiron site. Scheme 1 also depicts the proposed mechanism for reversible binding of O_2 (*1*−*3*).

Several lines of evidence [summarized by Brunhold and Solomon (*2, 6*)] show that the O_2 binding at the Hr/myoHr diiron site is best formulated as a concerted internal two-electron/one-proton transfer reaction:

$$[Fe1^{II}(\mu\text{-OH})Fe2^{II}] + O_2 \underset{k_{off}}{\overset{k_{on}}{\rightleftharpoons}} [Fe1^{III}(\mu\text{-O})Fe2^{III}O_2H^-] \quad (1)$$

The bound O_2 is, thus, formally a hydroperoxo ligand with its proton hydrogen-bonded to the oxo bridge. The O_2 association and dissociation rate constants, k_{on} and k_{off}, respectively, in reaction 1 can reflect not only Fe−O_2 bond formation/breakage, but also barriers to diffusional processes through the protein matrix and into the binding pocket implied in Scheme 1. Studies measuring O_2 affinities and association and dissociation rate constants have been published for several Hrs and myoHrs (*3, 7, 8*). With the exception of one early report (*9*), the O_2 association/dissociation reactions of Hrs exhibited monophasic kinetics, implying that any intermediate species, such as that shown in the center of Scheme 1, must be very short-lived at room temperature. The high O_2 association rate constants (10^7−10^8 M^{-1} s^{-1}) and low activation enthalpies for Hr and myoHr are consistent with rate-limiting diffusion of O_2 through the protein matrixes and/or opening of conformational "gates" leading to the O_2 binding pocket (rate-limiting diffusion through the solvent being ruled out by the lack of viscosity dependence) (*3, 7, 8, 10*−*12*). The O_2 dissociation rates have much higher activation enthalpies than for association, suggesting rate-determining bond breakage and/or substantial rearrangement of the metal coordination spheres.

Although the structure and function of the diiron site in Hr/myoHr is well established, the role of the protein matrix is less well characterized. Crystal structures are available for the oxy form of Hr (*1*), but only the met [autoxidized, diiron(III)] forms of myoHr (*5, 14*), in which either azide or chloride occupies the coordination position where O_2 binds in the oxy form (Fe2 in Scheme 1). The O_2 binding pocket of Hr/myoHr is lined with a set of conserved, hydrophobic residues, whose sequential positions are indicated in Figure 1. One or more side-chain atoms of residues I28, F55, W102, L103, and I107 lie within 4 Å of the coordinated O_2 atoms

† This work was supported by National Institutes of Health Grants GM 40388 (D.M.K.) and GM18865 (J.S.-L.).

* To whom correspondence should be addressed. Fax: 706-542-9454. E-mail: kurtz@sunchem.chem.uga.edu.

‡ University of Georgia.

§ Oregon Graduate Institute of Science & Technology.

10.1021/bi9929397 CCC: $19.00
Published on Web 06/27/2000

```
Tz_myoHr    1 GWEIPEPYVWDESFRVFYEQLDEEHKKIFKGIFDCIRD.N  39
               .:||||||||||||||||: ||:||| :|||:|.|  | .
Pg_myoHr1   1 PFDIPEPYVWDESFRVFYDNLDDEHKGLFKGVFNCAADMS  40
conserved             W           D H LF
                                     I

Tz_myoHr   40 SAPNLATLVKVTTNHFTHEEAMMDAAKYSEVVPHKKMHKD  79
              || ||   |: ||| || .||||||||||  |||||.||||
Pg_myoHr1  41 SAGNLKKLIDVTTTHFRNEEAMMDAAKYENVVPHKQMHKD  80
conserved         L          HF  E Y            H   H

Tz_myoHr   80 FLEKIGGLSAPVDAKNVDYCKEWLVNHIKGTDFKYKGKL 118
              || |:||| ||.|    :|| |:||| ||| |||||||||
Pg_myoHr1  81 FLAKLGGLKAPLDQGTIDYAKDWLVQHIKTTDFKYKGKL 119
conserved     F                     WL  HI   DF YKGKL
                                                  RI
```

FIGURE 1: Alignment of the amino acid sequences of Tz myoHr (Tz_myoHr, GenBank accession number P02247) and Pg myoHr isoform 1 (Pg_myoHr1, GenBank accession number P27686), and residues conserved in 10 different Hrs/myoHrs (conserved) (*4*). Symbols between the sequences indicate identities (|) and decreasing similarities (:, .) of residues. Conserved residues furnishing iron ligands are in black background, and conserved residues lining the O_2 binding pocket are in shaded background. Overlined residues of the Tz myoHr sequence are in helical regions (*5*).

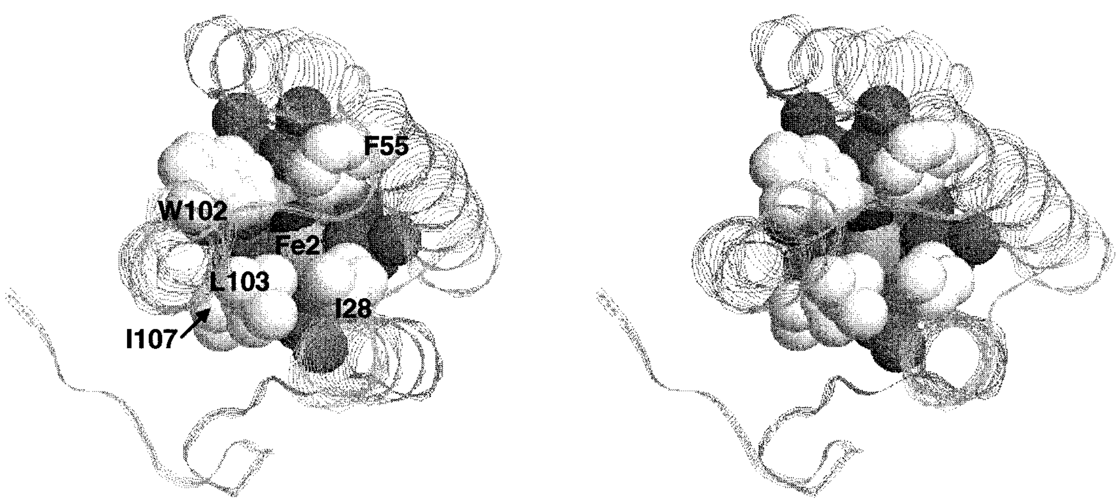

FIGURE 2: Stereoview of amino acid side chains lining the O_2 binding pocket in the azide adduct of Tz metmyoHr. Viewing perspective is approximately parallel to the long axis of the four-helix bundle and perpendicular to the Fe1−Fe2 axis (cf. Scheme 1). The protein backbone is shown in strand representation. Non-hydrogen atoms of amino acid side chains and heteroatoms are shown in space-filling representation. Residues lining the O_2 binding pocket are in lighter shade and labeled at their β-carbons. Iron ligand residues are in darker shade and to the rear of the pocket side chains in this view. Azide is omitted to expose its coordination site on Fe2. Drawings were generated with RASMOL (*13*) using coordinates from 2mhr in the Protein Databank (*5*).

in *T. dyscritum* (Td)[1] oxyHr, forming an O_2 binding pocket, as shown in Figure 2. It was proposed that one of these pocket residues, L103 in *T. zostericola* (Tz) myoHr, might limit access of small molecules to the O_2 binding pocket in that protein (*5, 14*). This proposal implies that k_{on} in reaction 1 would be limited by opening of a steric "gate" consisting of movement of specific residues that line the O_2 binding pocket. In principle the pocket residues could also slow O_2 dissociation by sterically hindering expansion of the Fe2 coordination sphere (cf. Scheme 1).

L103V and L103N mutants of Tz myoHr, intended to test the role of this residue, were found to autoxidize too rapidly to measure their O_2 association and dissociation rates (*15*). The autoxidation of Hr/myoHr can be formulated as either reaction 2a or 2b in which the hydroperoxide is displaced as H_2O_2 (*16*):

$$[Fe1^{III}(\mu\text{-}O)Fe2^{III}O_2H^-] + H^+ \rightarrow [Fe1^{III}(\mu\text{-}O)Fe2^{III}] + H_2O_2 \quad (2a)$$

$$[Fe1^{III}(\mu\text{-}O)Fe2^{III}O_2H^-] + H_2O \rightarrow [Fe1^{III}(\mu\text{-}O)Fe2^{III}OH^-] + H_2O_2 \quad (2b)$$

This reaction is relatively slow (half-time of several hours at room temperature) for the wild-type proteins. The rapid autoxidation of the L103 mutants of Tz myoHr relative to the wild-type protein can be explained by increased solvent access to the O_2 binding pocket (there being no endogenous

[1] Abbreviations: Tz, *Themiste zostericola*; Pg, *Phascolopsis gouldii*; Tricine, *N*-[2-hydroxy-1,1-bis(hydroxymethyl)ethyl]glycine; SDS−PAGE, sodium dodecyl sulfate−polyacrylamide gel electrophoresis; PCR, polymerase chain reaction; RT-PCR, reverse transcription-PCR; LB, Luria−Bertani medium; LB/amp, LB containing 100 μg/mL ampicillin; HEPES, 4-(2-hydroxyethyl)-1-piperazineethanesulfonic acid; LMCT, ligand-to-metal charge transfer; CD, circular dichroism; Tris, tris(hydroxymethyl)aminomethane; PCET, proton-coupled electron transfer.

Scheme 1

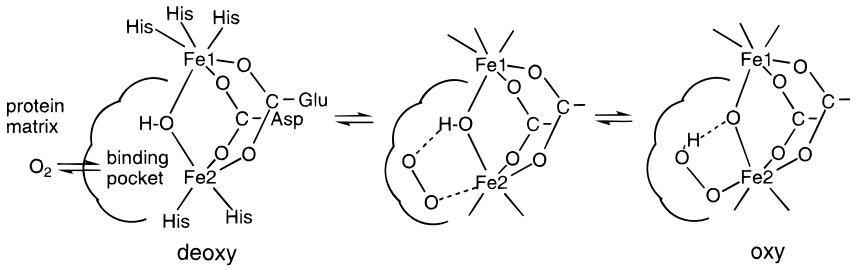

proton donor other than the hydroperoxide in the binding pocket of wild-type oxymyoHr). Since the met forms cannot bind O_2, autoxidation must be minimized in vivo in order to maintain functionality. The hydrophobic nature of the O_2 binding pocket residues in Hr and myoHr is, thus, rationalized. However, up to now no published work has directly examined the effects of changing pocket residues on k_{on} and k_{off} in the O_2 binding equilibrium of myoHr (reaction 1). The results described in this paper do so for L104 in *Phascolopsis gouldii* (Pg) myoHr1. This residue is analogous to L103 in Tz myoHr (cf. Figure 2). Pg myoHr1 has 70% sequence identity (77% similarity) to Tz myoHr; the helical secondary structure (judged by far-UV CD spectroscopy) and diiron site spectroscopic properties of Pg myoHr1 are indistinguishable from those of Tz myoHr (*17*).

EXPERIMENTAL PROCEDURES

Molecular biology procedures not described below followed those in Sambrook et al. (*18*), or in Ausubel et al. (*19*). Oligonucleotides were purchased from either Biopolymer Labs Inc. or Integrated DNA Technologies, Inc. Restriction enzymes were purchased from either Promega, Inc., or Boerhinger Mannheim, Inc. Nucleotide sequencing was carried out in the Molecular Genetics Instrumentation Facility at the University of Georgia. Protein overexpression was monitored by Tricine SDS−PAGE (*20*) on 1 mL samples of *E. coli* cultures before and after induction (as described below), and on cell-lysate fractions.

Cloning of the Pg myoHr Gene and Generation of Mutations. Specimens of *Phascolopsis gouldii* were obtained live from the Marine Biological laboratory, Woods Hole, MA. Muscle tissue was stripped from the inside of the body walls of approximately a dozen worms and centrifuged to give ~2.5 mL of tissue. This muscle tissue was suspended to ~7.5 mL in 4 M guanidinium thiocyanate and homogenized in an ice/water bath with a Polytron tissue homogenizer. RNA was isolated from the homogenized muscle tissue using a total RNA isolation kit from Stratagene, Inc. The cDNA encoding myoHr was isolated by RT-PCR of this total RNA using a Perkin-Elmer Cetus GenAmp RT-PCR kit. The N-terminal oligonucleotide primer used to amplify the cDNA had the sequence 5′-AGGAGATATACATATG-GGNTTYGAYATYCCRGARCCRTAYGTY-3′, that contained an *Nde*I restriction site (underlined) overlapping the start codon followed by a degenerate nucleotide sequence encoding the first nine residues of Pg myoHr isoform II (*17*). The N-terminal isoform II sequence differs from that of isoform I only at the N-terminal residue, which is glycine rather than proline (cf. Figure 1). This substitution was made in order to avoid possible inhomogeneity resulting from incomplete posttranslational N-terminal processing of the recombinant protein in *E. coli* (*21*, *22*). The complementary C-terminal oligonucleotide primer had the sequence 5′-ATGCAAGCTTANARYTTNCCYTTRTAYTT-3′, that contained a *Hin*dIII restriction site (underlined) overlapping a TAA stop codon, followed by a degenerate nucleotide sequence encoding the complement of the C-terminal six residues of Pg myoHr isoform I. The cDNA was amplified with these two primers by PCR using a thermal program consisting of 1 × 95 °C for 2 min, 35 × [42 °C for 1 min then 95 °C for 1 min], and 1 × 60 °C for 7 min. The resulting PCR product was inserted into the *Nde*I/*Hin*dIII sites of the polylinker in plasmid pT7-7 (*23*). The myoHr gene in the resulting plasmid, named pKD1-10, was found to encode an amino acid sequence identical to that of Pg myoHr isoform I, previously isolated from Pg muscle tissue (*17*), except for the substitution of the N-terminal proline by glycine. Site-directed mutagenesis of the myoHr gene was carried out using the splicing by overlapping extension (SOE) method (*24*) with pKD1−10 as template. Details of the SOE procedure and sequences of nucleotides used to introduce the mutations are provided in Supporting Information. All mutated plasmids were sequenced to verify introduction of the desired mutation.

Overexpression and Purification of Recombinant MyoHrs. Column chromatographies were run at room temperature. Gel filtrations were carried out on a Pharmacia Biotech FPLC system. Centrifugations and pressure ultrafiltrations were carried out at 4 °C. Plasmid pKD1-10 and its mutated derivatives were transformed into *E. coli* strain BL21(DE3) (Novagen, Inc.) (*25*). Induction of myoHr gene expression was accomplished as follows: *E. coli* BL21(DE3) (pKD1-10 or derivative) was inoculated into 50 mL volumes of LB/amp that were then incubated overnight in a 37 °C/250 rpm incubator/shaker. These 50 mL cultures were then used to inoculate 1 L batches of LB/amp, and incubation was continued at the same temperature and shaker speed. When the 1 L cultures reached an OD_{600} of ~1.0 (ca. 2 h), isopropyl-β-D-thiogalactopyranoside was added to a final concentration of 0.4 mM. Incubation was continued at 37 °C/250 rpm for 3−5 h until the OD_{600} reached ~2.1. The cells were harvested by centrifugation at 5000*g* for 5 min. The remaining procedure is described for the combined cell pellets from 6 L of *E. coli* culture. A modification of a published freeze/thaw method was employed to release myoHr from the cells (*26*). The cell pellet (25−30 g) was washed with buffer [50 mM Tris, 200 mM KCl (pH 8.0)], and the cells were re-isolated by centrifugation. The centrifuge bottles containing the pellet were placed in a −20 °C freezer for at least overnight or as long as a week.[2] The pellet

was then thawed gently in an ice/water bath as follows: approximately 150 mL of the same buffer was added to resuspend the pellet. Proteinase inhibitors were added to the following final concentrations: 2 mM EDTA, 0.5 μM PMSF, 1 μg/mL leupeptin, 5 μg/mL RNase A, and 20 μg/mL DNase I. The cell suspension was placed in an ice/water bath for as long as 3 h, during which it was intermittently agitated vigorously. After centrifugation at 30000*g* for 30 min, the pinkish or yellow supernatant was retained and the pellet was discarded. This supernatant contained the majority of the overexpressed myoHr (based on SDS−PAGE analysis). The supernatant was reduced to a volume of ∼5 mL in a 50 mL Amicon cell (YM-3 membrane, 3000 MWCO) under argon pressure, and then desalted by repeated concentration/redilution in the Amicon cell with 20 mM potassium phosphate (pH 7.0). The solution was centrifuged at 30000*g* for 10 min, and the supernatant was passed immediately over a QAE-Sephadex A-25 column in a 20 mL syringe barrel (Pharmacia Biotech). The column had been preequilibrated with 20 mM potassium phosphate (pH 7.0). The myoHr did not bind to the anion-exchange resin, and was eluted with the same buffer. The eluted pink or yellow fraction (∼10 mL) was collected and concentrated to a small volume (2−3 mL) in the Amicon cell. The concentrated sample was loaded onto a gel filtration column, either Superose 12 16/50 or Superdex 75 16/60, and eluted with 50 mM Tris-HCl and 200 mM KCl (pH 8.0) at a flow rate of 0.5 mL/min. Five-milliliter fractions were collected and analyzed by SDS−PAGE and UV−vis spectrophotometry. If necessary, the myoHr after gel filtration was subjected to a second anion-exchange column in order to remove traces of contaminating heme, which could be detected as a sharp absorption peak at ∼420 nm. The yield of wild-type or mutated myoHrs using this purification protocol was consistently ∼10 mg/L of *E. coli* culture (based on $\epsilon_{330} = 6500\ M^{-1}\ cm^{-1}$). The purified myoHrs were concentrated in a YM3 centricon concentrator (Amicon) and stored at either 4 °C for use within a few days or −80 °C for longer-term storage.

Preparation of Deoxy, Oxy, and Met Forms of MyoHrs. The buffer for all steps was 50 mM Tris, 200 mM KCl (pH 8.0). As-isolated myoHrs were usually mixtures of oxy and met forms. To convert the protein entirely to the met form, a small amount of solid potassium ferricyanide was added directly into the protein solution to a final concentration of ∼10 mM, and the mixture was allowed to equilibrate at 4 °C for more than 1 h. Excess potassium ferricyanide was then removed by dialysis against buffer in an Amicon cell with a YM-3 membrane. For preparation of the deoxy form, either the metmyoHr or the as-isolated myoHr (2−3 mL) was transferred into dialysis membrane tubing (3500 MWCO) and dialyzed anaerobically against 200 mL of degassed buffer containing a 10-fold molar excess of sodium dithionite. The dialysis was carried out at room temperature either in an anaerobic Coy chamber containing a N_2 atmosphere or under an argon atmosphere in a Schlenk-type sidearm flask connected to a vacuum manifold. The protein solution gradually turned colorless over the course of several hours or longer, indicating reduction to the deoxy form. Excess sodium dithionite was removed by extensive dialysis against dithionite-free buffer under the same anaerobic conditions. Upon reexposure to air, the protein solution immediately turned a pink−red color, indicating formation of oxymyoHr, or for some of the mutated myoHrs, turned yellow, indicating rapid autoxidation. The deoxy- or oxyproteins were either immediately subjected to optical or kinetic characterizations, or stored at −80 °C. Azide binding was achieved by adding sodium azide to a final concentration of 50 mM (>100-fold molar excess) to metmyoHr solutions and allowing the mixture to equilibrate overnight at room temperature.

Measurement of O_2 Binding Affinities and Kinetics for Recombinant MyoHrs. All data were collected for solutions of myoHr in 50 mM Tris, 200 mM KCl, pH 8.0. All reported data are the averages of at least three determinations. O_2 affinities for wild-type and mutated myoHrs were measured by spectrophotometric tonometry at room temperature. The method has been previously described for Pg Hr (*27*). Solutions of deoxymyoHr to be examined (∼1.5−3 mL, ∼0.5−1 mM) were transferred to a specially adapted 1 cm path length cell and attached to the tonometer. The O_2 association constant was expressed as P_{50}, the partial pressure of O_2 at which $[\text{oxymyoHr}]/[\text{myoHr}]_{total} = 0.5$, as determined from exponential fits to plots of A_{500} vs P_{O_2}.

Measurements of the O_2 dissociation rates for the Pg oxymyoHrs were carried out on an RSM-1000 stopped-flow spectrophotometer fitted with a rapid-scanning monochromator (OLIS, Inc.). The method follows that previously used on Tz myoHr (*3*, *8*). OxymyoHr solutions placed in one drive syringe of the stopped-flow instrument were rapidly mixed with a sodium dithionite solution from the other drive syringe, which rapidly scavenges dissolved O_2. The concentrations after mixing were 22.5 mM sodium dithionite and 20−100 μM deoxymyoHrs. After the mixing dead time (∼2 ms), visible spectra over the range of 360−600 nm were acquired every millisecond until 0.5−14 s depending on the individual experiment. Alternatively, the decrease of absorbance at a single wavelength (500 nm) vs time was recorded continuously. Rate constants for O_2 dissociation were determined by fitting the decrease in absorbance at 500 nm vs time to a first-order exponential decay. The temperature dependences of the O_2 dissociation rates were determined on the same stopped-flow spectrophotometer, which was equipped with a thermostated water bath. The activation parameters were determined from Eyring plots with at least four data points in the range of 5−25 °C. Measurements of deuterium isotope effects on the O_2 dissociation rates for the wild-type, L104F, and L104Y myoHrs were carried out in D_2O buffer. The D_2O buffer was prepared as follows: a small volume of concentrated hydrogen chloride was diluted with 10 mL of D_2O (99.8%, Aldrich Chemical Co.) and was used to adjust the pD of 50 mL of 50 mM Tris dissolved in D_2O to 8.0. The solution was rotary-evaporated to dryness in a SpeedVac concentrator (Savant, Inc.) and then redissolved in 50 mL of D_2O. Potassium chloride was added to a final concentration of 200 mM.

O_2 association rates of the myoHrs were measured under pseudo-first-order conditions (excess O_2) on the same OLIS stopped-flow spectrophotometer as used for O_2 dissociation rates. One drive syringe of the stopped-flow spectrophotometer was deoxygenated by incubation with sodium dithionite solution (20 mM) for at least 30 min followed by washing

[2] Freezing at −80 °C resulted in release of additional cellular components upon thawing, which interfered with subsequent purification.

with degassed dithionite-free buffer. DeoxymyoHr solution was transferred anaerobically into this syringe under an argon flow. The other drive syringe was filled with air-saturated buffer. Upon rapid mixing of the two solutions, the increase in absorbance centered at 500 nm was monitored either by the rapid-scanning procedure or at fixed wavelength (500 nm). After mixing, the protein concentration was typically 15−20 μM, and the O_2 concentration was typically 0.1−0.2 mM as estimated by using a YSI model 5300 biological oxygen monitor. Plots of absorbance at 500 nm versus time were fitted to a first-order exponential function. The activation parameters for O_2 association were also determined by temperature-dependent rate measurements between 4 and 25 °C.

Autoxidation rates of oxymyoHrs (reaction 2) were measured under ambient air and room temperature (23−25 °C) by monitoring the decrease in absorbance at 500 nm vs time on a Shimadzu UV2101PC UV−vis spectrophotometer. The data were fitted to a first-order exponential function to obtain the half-time of the autoxidation, $t_{1/2}$. For those myoHrs that autoxidized too rapidly for this procedure, A_{500} vs time was monitored by mixing solutions of the deoxymyoHr with O_2 solution in the OLIS stopped-flow spectrophotometer, as described for measuring O_2 association rates.

Spectroscopy. Electronic absorption spectra of myoHrs were obtained at room temperature on a Shimadzu UV2101PC spectrophotometer. Far-UV CD spectra were recorded on a Jasco 710 CD spectrometer equipped with a nitrogen purge. The CD amplitude was calibrated with a standard androsterone solution. MyoHr samples of 20−40 μM were measured in a cylindrical quartz cuvette of 0.01 cm path length. All spectra were obtained at 25 °C in 50 mM phosphate buffer (pH 7.5), and five or more scans were averaged for each sample.

Resonance Raman spectra were obtained on myoHr samples shipped frozen in dry ice to the Oregon Graduate Institute. Spectra were obtained either at ice temperature (oxy and met forms) or at 15 K (azidomet forms) using a 90° scattering geometry on a McPherson 2061 spectrograph with an 1800 groove grating and a Princeton Instruments liquid N_2 cooled (LN100PB) CCD detector. The excitation sources were a Coherent INNOVA 300 Kr^+ laser for 413.1 nm and a Spectra Physics Ar^+ 164 laser for 514.5 and 488.0 nm. Raman samples were 1−2 mM in protein (per 2Fe) and in 50 mM HEPES and 150 mM Na_2SO_4, pH 7.5.

RESULTS

Molecular and Spectroscopic Properties of the Recombinant MyoHrs. Overexpression of the wild-type Pg myoHr gene in *E. coli* BL21(DE3)[pKD1-10] yielded a soluble, diiron-containing protein that could be purified to homogeneity in reasonably good yield (~10 mg/L of culture) from the supernatant of freeze/thaw-lysed cells in two successive chromatographic steps. The analogous protocol gave similar yields of L104X Pg myoHrs. The as-purified myoHrs were usually mixtures of oxy and met forms based on the distinctive and characteristic absorption spectra of the two forms (see below). We found that not all mutated Pg myoHrs were overexpressed in this system. Pg myoHr genes encoding L104V, -F, -Y, -T, and -N produced properly folded, soluble proteins (see below). However, repeated attempts at overexpression of L104A, -W, -H, and -D did not yield any detectable myoHr-like proteins, either in the lysed-cell supernatant or as inclusion bodies in the lysed cell pellet. All of the overexpressed myoHrs were found to be monomeric by gel filtration.

The CD spectra of Pg recombinant wild-type, L104Y, and L104F metmyoHrs were recorded and are included as Supporting Information. All three spectra are virtually identical to each other and have double minima at 208 and 222 nm and an average molar ellipticity at 222 nm ($[\theta]_{222}$) of −23 000 deg cm^2/dmol. These features are characteristic of proteins with predominantly helical secondary structure and closely resemble those in the CD spectra of metmyoHrs isolated from both Pg and Tz (*28*, *29*). Using the measured molar ellipticity with a conventional method (*28*), a ~70% helix content was calculated for all three of these recombinant Pg myoHrs. This percentage agrees very well with that determined by X-ray crystallography of other Hrs and myoHrs (*1*, *5*). As shown in Figure 2, the diiron site effectively cross-links the four-helix bundle. Therefore, the far-UV CD data, together with the UV−vis absorption and Raman spectra (discussed below) showing preservation of the diiron site, demonstrate that the native four-helix bundle structure is retained in the recombinant wild-type and L104X Pg myoHrs.

Figure 3 displays the UV−vis absorption spectra for met, oxy, and azidomet forms of the wild-type and L104X Pg myoHrs. The A_{280}/A_{330} absorbance ratio for the recombinant wild-type Pg metmyoHr was determined to be 3.8, which is slightly lower than the value of 4.3 reported for the native Pg metmyoHr (*17*), presumably indicating a higher purity for the recombinant protein. All of the L104X metmyoHrs had A_{280}/A_{330} absorbance ratios of ~4. These absorbance ratios indicate full iron occupancy of the diiron sites. The UV−vis absorption spectra of the met forms of L104V, -F, and -Y myoHrs are virtually identical to that of the wild type. The absorption features at ~320 and ~360 nm, and shoulder at ~480 nm, are due to μ-oxo→Fe(III) LMCT transitions and serve as fingerprints for μ-oxo-diiron(III) sites (*30*). The small difference in the relative intensities of the 320 and 360 nm absorbances for L104N and L104T metmyoHrs relative to the others is probably due to increased solvent occupancy in the ligand binding pockets of these polar-residue-mutated L104X myoHrs (*14*).

Of the Pg myoHrs we prepared, the wild-type and L104V, -F, and -Y yielded oxy forms that were reasonably stable against autoxidation ($t_{1/2}$ > 30 min at room temperature). Here again, the absorption spectra of the L104X oxymyoHrs are essentially identical to that of the wild type and characteristic of the O_2 adduct. In addition to the peak at 330 nm and shoulder at ~360 nm [both due to oxo→Fe(III) LMCT], all of these myoHrs displayed a broad absorption centered near 500 nm, which is due to the hydroperoxo→Fe(III) LMCT transition (*30*). Similarly, spectra of the azide adducts of the mutated metmyoHrs are essentially identical to that of the wild type, displaying absorption maxima near 326, 380, and 445 nm. The lowest energy absorption feature is due to azide→Fe(III) LMCT. The L104N and L104T metmyoHr azide adducts appear to be incompletely formed, which is consistent with competing solvent in the ligand binding pocket, as suggested above.

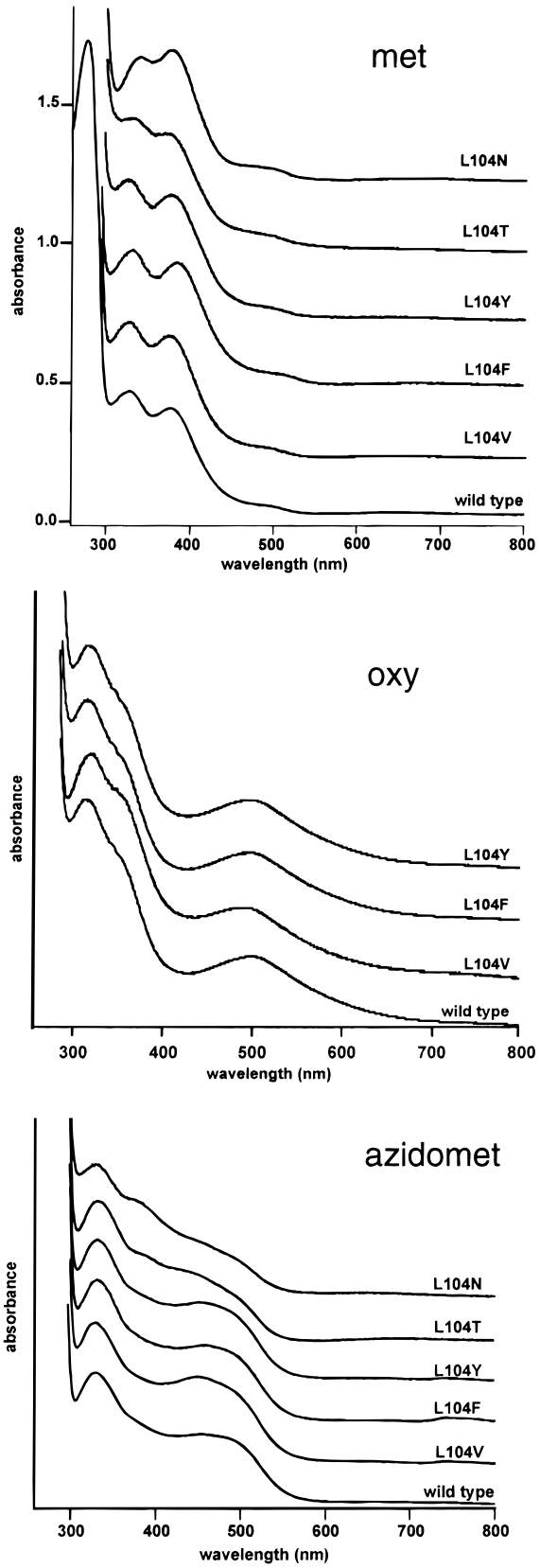

FIGURE 3: UV−vis absorption spectra of recombinant wild-type and L104X Pg met (top panel), oxy (middle panel), and azidomet (bottom panel) myoHrs. Spectra within each panel are normalized to equal absorbance at 280 nm and offset vertically by an arbitrary amount for clarity. All spectra were obtained at room temperature in 50 mM Tris and 200 mM KCl, pH 8.0. Azide adducts were prepared by addition of sodium azide to 50 mM (~100-fold molar excess over diiron sites), and were allowed to react for several hours at room temperature before recording spectra.

Table 1: Resonance Raman Frequencies of Diiron Sites in Hrs and MyoHrs[a]

Hr or myoHr	ν(O−O)	ν(Fe−O_2)	ν_s(Fe−O−Fe)	ν(Fe−N_3)-[ν_{as}(N_3)]
Pg wt[b] oxymyoHr	844 (+2)	503 (−2)	485 (+5,+37)[c]	−
Pg L104Y oxymyoHr	844 (+2)	502 (−2)	477 (+5,+28)[c]	−
Pg oxyHr[d]	844 (+4)	503 (−3)	486 (0)	−
Pg wt[b] metmyoHr	−	−	505 (0)	
Pg L104Y metmyoHr	−	−	509(+9)	−
			492 (+8)	
Pg L104F metmyoHr	−	−	505 (0)	−
Pg metHr[d]	−	−	510 (0)	−
Tz metmyoHr[e]	−	−	507	−
Pg wt[b] azido-metmyoHr	−	−	513	373 [2049]
Pg L104F azido-metmyoHr	−	−	513	375 [nd][f]
				340
Pg L104Y azido-metmyoHr	−	−	510	372 [2052]
Pg azidometHr[d]	−	−	507	375 [2048]
Tz azidomet-myoHr[e]	−	−	507	376 [2050]

[a] Frequencies (D_2O shifts) in cm^{-1}. All data for Pg myoHrs are from this work. Frequencies in italics represent minor components. [b] Wild type. [c] Frequencies are estimated from deconvolution of overlapping bands. The two frequencies in D_2O are attributed to Fermi resonance (*33*). [d] From Shiemke et al. (*31*). [e] From Duff et al. (*32*). [f] Not determined.

Resonance Raman spectra were obtained of met, azidomet (Figure 4), and oxy (Figure 5) forms of recombinant wild type and L104F and L104Y Pg myoHrs. Table 1 collects the observed Raman frequencies and assignments and compares our data with previously published resonance Raman data on Pg Hr and Tz myoHr. Using 413 nm laser excitation, which selectively enhances the $Fe^{III}-O^{2-}-Fe^{III}$ vibrational modes (*31, 33*), the wild-type metmyoHr exhibited a ν_s(Fe−O−Fe) frequency of 506 cm^{-1}. For L104Y metmyoHr, two overlapping peaks in the ν_s(Fe−O−Fe) region were observed and deconvoluted by curve fitting. The major fitted component at 509 cm^{-1} was 3 cm^{-1} upshifted from the wild-type frequency and showed a large upshift in D_2O (cf. Table 1). A minor component fitted at 492 cm^{-1} showed a similarly large D_2O upshift. We attribute these effects to the introduction of the hydroxyl of Y104 into the binding pocket, where it either hydrogen bonds to the oxo bridge or recruits solvent molecules. Neither the UV−vis nor the resonance Raman spectra of L104YmetmyoHr showed the characteristic and readily detectable spectral signatures of Fe(III)−tyrosinate ligation (*34, 35*). The azide adducts of wild-type and L104Y metmyoHrs showed the characteristic Raman frequencies for an azido ligand end-on-coordinated to Fe2 (cf. Figure 4 and Table 2) (*31*). The L104F azidometmyoHr showed two ν(Fe−N_3) bands, presumably representing two slightly different geometries of azide coordination. Only one ν_s(Fe−O−Fe) band was observed for L104F azidometmyoHr. These resonance Raman spectra indicate very similar diiron site structures for the met and azidomet forms of Pg wild-type, L104F, and L104Y myoHrs and that these structures closely resemble those in other Hrs (cf. Table 1).

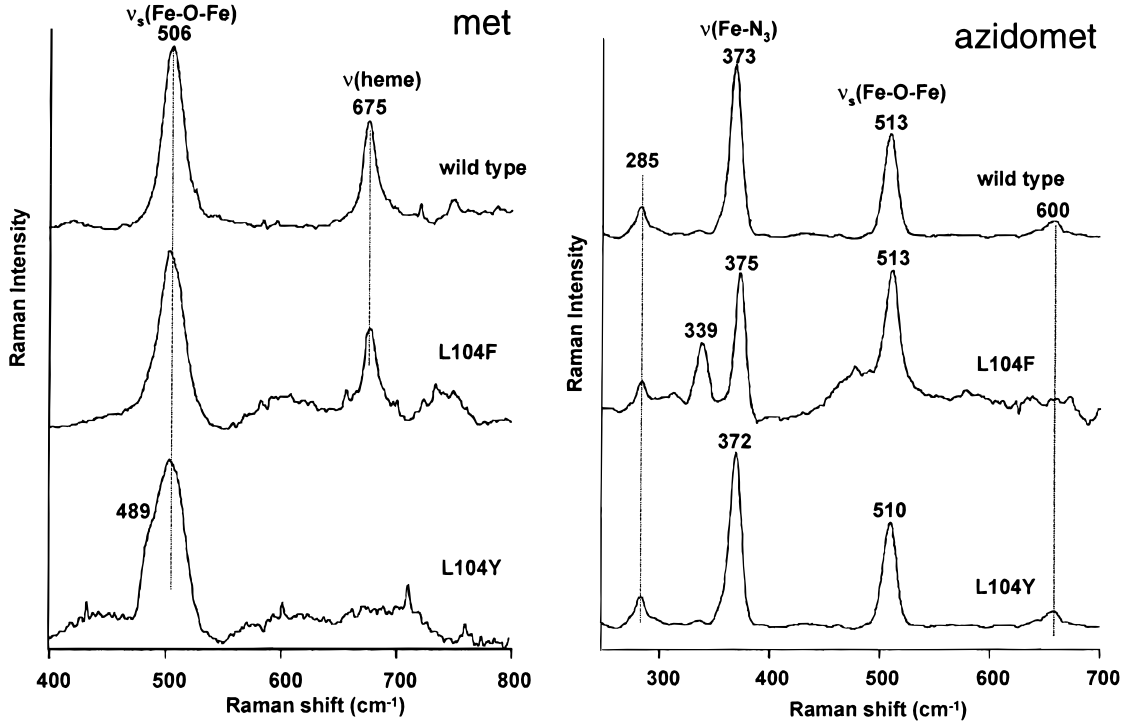

FIGURE 4: Resonance Raman spectra of recombinant wild-type, L104F, and L104Y Pg met- and azidometmyoHrs. MetmyoHr spectra (left panel) are in the ν_s(Fe−O−Fe) region and were obtained in 50 mM HEPES,150 mM Na_2SO_4, pH 7.5, with the following spectral conditions: 413 nm laser excitation, 20 mW @ sample, ice temperature, 90° scattering, aspirin standard, 10 min excitation. The 675 cm^{-1} feature labeled ν(heme) is due to a very small amount of contaminating heme. AzidometmyoHr spectra (right panel) are in the ν(Fe−N_3) stretching region and were obtained in the same buffer as for the met samples but with sodium azide added to 50 mM and the following spectral conditions: 514.5 nm laser excitation, 60 mW @ sample, temperature = 15 K, 150° scattering, aspirin standard, 5 min scans.

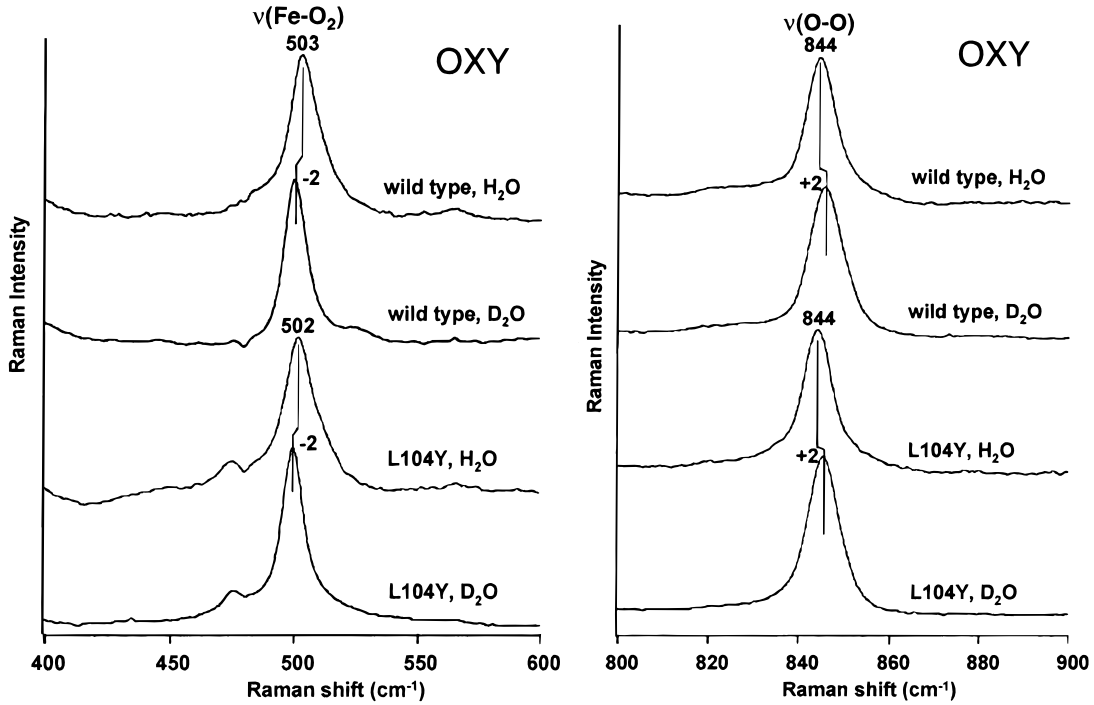

FIGURE 5: Resonance Raman spectra of recombinant Pg wild-type and L104Y oxymyoHrs in the ν(O−O) (right panel) and ν(Fe−O_2) (left panel) stretching regions. Conditions: H_2O or D_2O buffer (50 mM HEPES, 150 mM Na_2SO_4, pH or pD 7.5), 514.5 nm laser excitation, 10 mW @ sample with a 10 min exposure time, ice temperature, 90° scattering, aspirin standard.

Resonance Raman spectra were also recorded for oxy forms of recombinant wild-type and L104Y Pg myoHrs (Figure 5). Using 514 nm laser excitation, which selectively enhances the $Fe2^{III}-O_2H^-$ modes (*31*), both the wild-type and L104Y oxymyoHr showed a ν(O−O) peak at 844 cm^{-1} and a ν(Fe−O_2) peak at 503−504 cm^{-1} in their resonance Raman spectra. In D_2O buffer, the ν(O−O) at 844 cm^{-1} showed a 2 cm^{-1} upshift for both myoHrs. These frequencies for ν(O−O) and ν(Fe−O_2) as well as the frequency upshifts in D_2O closely resemble those previously reported for oxyHr

Table 2: Kinetic and Equilibrium Data for O_2 Binding to Recombinant Pg MyoHrs[a]

myoHr	P_{50} (mmHg)	k_{off} (s^{-1})	$\Delta H^{\ddagger}_{off}$ (kcal/mol)	$\Delta S^{\ddagger}_{off}$ (cal mol^{-1} K^{-1})	k_{on} ($\times 10^5$ M^{-1} s^{-1})	$\Delta H^{\ddagger}_{on}$ (kcal/mol)	$\Delta S^{\ddagger}_{on}$ (cal mol^{-1} K^{-1})	autoxidation $t_{1/2}$
wild type	2.2 ± 0.2	240 ± 5 (190 ± 6)[b]	20.4 ± 0.8	20 ± 3	>700	–	–	10 h
L104V	2.6 ± 0.5	130 ± 3 (110 ± 5)[b]	18.8 ± 0.5	14 ± 2	>700	–	–	3 h
L104F	1.5 ± 0.2	1.8 ± 0.1 (1.6 ± 0.1)[b]	29 ± 1	40 ± 1	7 ± 2	4 ± 1	-37 ± 3	5.5 h
L104Y	1.2 ± 0.2	0.58 ± 0.02 (0.45 ± 0.01)[b]	29 ± 1	34 ± 4	3.6 ± 0.5	7 ± 2	-27 ± 8	11 h
L104N	–	–	–	–	–	–	–	1.2 s
L104T	–	–	–	–	–	–	–	<2 ms
F56Y	–	–	–	–	–	–	–	6 s
W103A	–	–	–	–	–	–	–	<2 ms
W103F	–	292 ± 9	20 ± 2	20 ± 6	>700	–	–	0.5 h

[a] Conditions: 50 mM Tris, 200 mM KCl, pH 8.0 at 25 °C; activation parameters were determined from rates obtained between 5 and 25 °C. [b] Values in parentheses were determined in D_2O buffer.

(*31*, *33*). Using 413 nm excitation, the ν_s(Fe−O−Fe) oxo-bridge bands for wild-type and L104Y oxymyoHrs were also observed. These spectra are contained in the Supporting Information. Interpretation of these latter spectra was complicated by the fact that the concentrated myoHr samples were invariably contaminated with the met form due to autoxidation. By comparison with the spectra of the fully met forms in Figure 4 and deconvolution by curve-fitting, the tentative assignments of ν_s(Fe−O−Fe) for the oxymyoHrs listed in Table 1 have been made. Even without deconvolution, it is apparent qualitatively that the ν_s(Fe−O−Fe) frequencies of wild-type and L104Y oxymyoHrs differ by no more than a few cm^{-1}. Surprisingly, resonance Raman data have been previously reported on oxy forms of octameric Hrs but apparently not on any oxymyoHr (*7*).

Kinetics and Equilibria of O_2 Binding and Autoxidation. Kinetics and equilibrium data for O_2 binding (reaction 1) and autoxidation (reaction 2) for the wild-type and the five L104X Pg myoHrs are collected in Table 2. O_2 affinities are reported as P_{50}, the O_2 partial pressure at which a 50:50 mixture of the oxy and deoxy forms is attained. The P_{50} values are inversely proportional to the O_2 association equilibrium constants. For O_2 association and dissociation rates, k_{on} and k_{off}, respectively, the activation parameters derived from the temperature dependences are also reported. All solutions were buffered at pH 8.0. The pH dependences of the reactions were not examined; O_2 binding kinetics and equilibria for other Hrs and myoHrs have previously been reported to be pH-independent between pH 6 and 9 (*3*, *36*). For those autoxidations that were slow enough ($t_{1/2} \geq 30$ min at 25 °C) to be monitored by conventional scanning spectrophotometry, the overlaid set of scans (not shown) showed an isosbestic point near 430 nm, which is consistent with direct conversion of the oxy to the met form according to reaction 2. Faster autoxidations were monitored by stopped-flow starting from the deoxy form. More detailed kinetics data are included in Supporting Information.

O_2 Association and Equilibria. Three of the five L104X myoHrs examined, L104V, -F, and -Y, formed stable O_2 adducts at room temperature. The two mutations to residues with larger side chains, namely, Y and F, gave myoHrs exhibiting the most dramatic perturbations of the O_2 dissociation rates, ~400-fold slower for L104Y and ~130-fold slower for L104F (cf. Table 2). L104V myoHr behaved similarly to the wild type with only an ~2-fold decrease in the O_2 dissociation rate. O_2 affinities of L104V, L104F, and L10Y myoHrs were all close to that of the wild type. The combined data on O_2 dissociation rates and O_2 affinities predict a decrease in O_2 association rates of 2-fold, 100-fold, and 250-fold, respectively, for L104V, L104F, and L104Y myoHrs, assuming that the equilibrium O_2 affinities can be equated with k_{on}/k_{off}. We found that the O_2 association rates for the wild-type and L104V Pg myoHrs were too fast to measure by stopped-flow spectrophotometry, as is the case for Tz myoHr (*8*). However, the predicted decreases in the O_2 association rates for L104F and L104Y myoHrs suggested that we might be able to measure the O_2 association rates directly by rapid mixing of O_2 solutions with the deoxy protein in the stopped-flow spectrophotometer. This suggestion was borne out by experiment. The second-order O_2 association rates for L104F and L104Y myoHrs were determined by the stopped-flow method to be 7×10^5 and 3.6×10^5 M^{-1} s^{-1}, respectively. These rates were determined from absorbance increases at 500 nm, and also from scanning stopped-flow spectrophotometry from 350 to 650 nm. The kinetic traces from either method showed no evidence for a multiphasic process or for a process occurring faster than the stopped-flow time scale; i.e., no chromophoric intermediates in the O_2 association process could be detected. The agreement between calculated and observed O_2 association rates confirms that our kinetics and equilibrium measurements can be reliably compared and *that they are measuring the same processes*. Our estimated value of the O_2 association rate for wild-type Pg myoHr (calculated from the measured k_{off} and P_{50}) is $\sim 8 \times 10^7$ M^{-1} s^{-1}, i.e., on the order of 100 times faster than for L104F and L104Y Pg myoHrs. This estimated value of k_{on} for wild-type Pg myoHr agrees very well with that obtained for Tz myoHr from temperature jump measurements (*8*), but is ~60 times higher than the k_{on} of 1.4×10^6 M^{-1} s^{-1} determined from laser-flash photolysis of Tz oxymyoHr (at 21.5 °C rather than 25 °C) (*3*). We suggest that the latter rate constant, which was determined from small A_{500} changes triggered by a green laser flash, does not reflect the spontaneous, second-order O_2 association process for deoxymyoHr at or near room temperature.[3] Based on the P_{50} and k_{off} values in Table 1, the second-order O_2 association rate constant for L104V myoHr must be similar to that of the wild type.

O_2 Dissociation. The O_2 dissociation rate and corresponding activation parameters measured in this study for wild-type Pg oxymyoHr are close to those reported for Tz oxymyoHr, which were measured by the same stopped-flow method (*3, 8*). The much lower O_2 dissociation rates for L104F (130-fold) and L104Y (400-fold) Pg myoHrs relative to wild type are reflected in significantly higher $\Delta H^{\ddagger}_{off}$ values (Table 2). The $\Delta S^{\ddagger}_{off}$ values are also significantly higher for L104F and -Y myoHrs, and these changes in activation parameters presumably reflect a mechanistic alteration. The L104N and L104T Pg myoHrs autoxidized too rapidly to measure k_{off}. The D_2O isotope effect (k_{H2O}/k_{D2O}) on the O_2 dissociation rate of the wild-type Pg myoHr was determined to be 1.3 at 25 °C, which is similar to the reported values for O_2 dissociation in Pg Hr (1.2) (*37*) and Tz myoHr (1.6) (*3*). These isotope effects are consistent with a mechanism in which transfer of the proton from hydroperoxide ligand to the oxo bridge (cf. Scheme 1) contributes only a small portion of the activation barrier to O_2 dissociation. The D_2O isotope effects for L104F and -Y, 1.1 and 1.3, respectively, were similar to that for the wild-type oxyHr.

Autoxidation. The autoxidations (reaction 2) of L104F and L104Y Pg oxymyoHrs ($t_{1/2}$ = 5.5 and 11 h, respectively) were only marginally different from that of wild type ($t_{1/2}$ = 10 h) at 25 °C. L104V Pg myoHr showed an approximate 3-fold increase in autoxidation rate ($t_{1/2}$ = 3 h),[4] whereas the autoxidation rate for L104N Pg myoHr was much faster, $0.56 \pm 0.1\ s^{-1}$ ($t_{1/2} \sim 1.2$ s). The autoxidation rate for L104T myoHr was too fast to measure by stopped-flow spectrophotometry, and, must, therefore, be complete in less than 2 ms under our conditions.

DISCUSSION

The molecular and spectroscopic comparisons to the wild type indicated that both the monomeric four-helix bundle and the diiron site structures were preserved in the L104 Pg myoHrs. In those cases where the L104X myoHr could be overexpressed, the mutations induced little or no detectable perturbations of the diiron sites, whether in the met, azidomet, or oxy forms. Nevertheless, all of the overexpressed L104X myoHrs showed significant perturbations in their reactivity with O_2. These perturbations in reactivity must then be due to alterations in the O_2 binding pocket rather than in the diiron site$-O_2$ complex itself.

Substitution of L104 with aromatic residues (F or Y) resulted in a ≥100-fold *decrease* in k_{on}. These slower rates could be construed to indicate that L104 functions as a steric "gate" whose movement allows O_2 access to the binding pocket in the rate-determining step for O_2 association. However, if so, then one would expect that substitution with the smaller valine side chain in L104V would result in a significant *increase* in the O_2 association rate, whereas we estimate little or no perturbation of the O_2 association rate in this mutant. *Thus, our results indicate that L104 does not function as a "gate" to the binding pocket during the rate-determining step of O_2 association to the myoHr*. This conclusion is consistent with the second-order rate constant of $\sim 8 \times 10^7\ M^{-1}\ s^{-1}$ for O_2 association in wild-type myoHrs being controlled by diffusion through a rapidly fluctuating protein matrix. Preferred diffusional pathways through the protein matrix for productive "attack" on the diiron site may lower the O_2 association rate below that estimated for diffusion-controlled encounter of a small molecule with a protein ($\sim 10^9\ M^{-1}\ s^{-1}$) (*38*, *39*). Such a rate-determining step is consistent with the small, positive activation volume observed for the O_2 association reaction of Hr, which was attributed to "dynamic breathing" of the protein (*40*). The $\Delta H^{\ddagger}_{on}$ values of 4 and 7 kcal/mol for the L104F and L104Y Pg myoHrs, respectively, are still much lower than one would expect for a dissociative mechanism at Fe2 (such as might occur if solvent were coordinated to Fe2 in the deoxy form). Furthermore, these slower O_2 association reactions were not accompanied by formation of any detectable intermediate species. We, therefore, attribute the significantly slower O_2 association rates for L104F and L104Y Pg myoHrs to introduction of a dynamic, steric barrier consisting of an aromatic side chain that partially fills vacant space either in the O_2 binding pocket or along a productive O_2 diffusional pathway. The O_2 dissociation data on these same mutants (vide infra) suggest that a steric barrier has been introduced at the binding pocket in these mutants.

The lack of any detectable chromophoric intermediate during O_2 association with deoxymyoHr, even when this reaction is slowed by 2 orders of magnitude as in L104F and -Y, is consistent with a mechanism in which an oxidized diiron site intermediate does not accumulate to any appreciable extent. Brunhold and Solomon (*2*) have in fact proposed a concerted proton/electron-transfer mechanism *following* the initial O_2 binding to Fe2 in deoxyHr, in which an intermediate, such as that shown in Scheme 1, would *not* accumulate. If either diffusion through the protein matrix or steric restrictions in the binding pocket limit O_2 association, then the concerted proton/electron transfer must occur *after* the rate-determining step. The lack of *any* detectable deuterium isotope effect on the O_2 association rate for Hr (*37*) is consistent with these conclusions.

Positive activation volumes, much larger than those for O_2 association, have previously been measured for O_2 dissociation from Tz oxymyoHr (*3*) and Pg oxyHr (*40*), and these were interpreted as indicating expansion of the Fe2 coordination sphere in the transition state (cf. Scheme 1). This mechanism is consistent with the 130- and 400-fold slower O_2 dissociation rates that we observed for L104F and L104Y Pg oxymyoHrs (cf. Table 2), respectively; that is, the larger side chains inhibit expansion of the Fe2 coordination sphere. The essentially unperturbed UV−vis and resonance Raman spectra of L104Y oxymyoHr relative to those of wild-type protein indicate that neither structural nor electronic alterations of the diiron site are responsible for the slower rates. The similarly small D_2O isotope effects on the O_2 dissociation rates of L104V, L104F, and L104Y myoHrs also indicate that the proton-transfer contribution to the O_2 dissociation rate, including that conceivably arising from the Y104 hydroxyl, is still small in the L104X myoHrs.

[3] Under our stopped-flow experimental conditions and concentrations, a k_{on} of $1.4 \times 10^6\ M^{-1}\ s^{-1}$ would result in an ΔA_{500} with a pseudo-first-order rate constant of $\sim 20\ s^{-1}$, which we could have readily measured. In fact, we found that the wild-type Pg myoHr O_2 association reaction was essentially complete within the mixing time (~2 ms) at 25 °C, which sets a lower limit of $\sim 7 \times 10^7\ M^{-1}\ s^{-1}$ for the O_2 association rate constant.

[4] This autoxidation half-time is ~20 times slower than that reported for L103V Tz myoHr (*15*); we have no convincing explanation for this difference.

Here again, if L104 in the wild-type protein were inhibiting expansion of the coordination sphere during O_2 dissociation, then we would expect the L104V myoHr to exhibit an increase in the O_2 dissociation rate, when, in fact, k_{off} decreases slightly for this mutant. *Therefore, we conclude that L104 does not provide any special barrier or "gate" which inhibits O_2 dissociation in oxymyoHr*.

Assuming that autoxidation of oxymyoHr (eq 2) is rate-limited by solvent access to the O_2 binding pocket, our results show that mutations to larger and aromatic residues at L104 do not significantly affect solvent access. Given the apparently increased crowding of the L104F and -Y binding pockets indicated by the O_2 association and dissociation rates, the very minor perturbations of the autoxidation rates by these mutations strongly suggest the absence of any significant water occupancy in the wild-type oxymyoHr O_2 binding pocket. This conclusion is consistent with the X-ray crystal structure of oxyHr, which shows no solvent occupying its O_2 binding pocket (*1*). A relatively minor increase in autoxidation rate was observed upon substitution with the smaller nonpolar residue, V, for L104. Much more dramatic increases in the autoxidation rate were observed when polar residues of approximately the same size as valine, namely, N or T, were substituted for L104. The $>10^6$ times faster autoxidation of L104T over L104V suggests that polarity much more so than size of the side chain modulates water occupancy, and, thereby, the autoxidation rate. Thus, for autoxidation, L104 may function as a "gate", but the activation barrier is predominantly hydrophobic rather than steric. This line of reasoning reflects the suggestion of Feher et al. (*38*) that polarity rather than size limits diffusion of small molecules, including water, into buried, hydrophobic cavities within proteins. *Thus, a hydrophobic residue 104 in Pg myoHr inhibits autoxidation.*

Our most significant conclusions and proposals about the roles of the conserved O_2 binding pocket residue 104 in Pg myoHr are listed below:

(i) Our results are consistent with the following rate-limiting processes in the wild-type (L104) protein: O_2 diffusion through a fluctuating protein matrix for association, expansion of the Fe2 coordination sphere for O_2 dissociation, and solvent entry into the binding pocket for autoxidation.

(ii) L104 provides no special barrier to O_2 diffusion or entry into the binding pocket, nor does it provide a significant steric barrier during the rate-determining step of O_2 dissociation. The leucine side chain appears to have close-to-optimal properties for its position at the binding pocket: it is nonprotic, non-oxidizable, sufficiently hydrophobic to inhibit autoxidation, but small enough not to sterically inhibit O_2 association or dissociation.

(iii) Artificial activation barriers to both O_2 association and dissociation can be introduced by substitution of aromatic residues (F or Y) for L104. These barriers appear to be steric in nature, most likely due to partial filling of the binding pocket, and do not result in stabilization of any chromophoric intermediate species. The fact that O_2 still binds to these mutants implies a limited flexibility of the binding pocket.

Our kinetic results on O_2 binding pocket leucine mutants of an octameric Hr have led us to conclusions similar to those described here for myoHr (*41*). The evolutionary 'optimization' of L104 presumably occurred in concert with the other binding pocket residues shown in Figure 2. We have carried out analogous studies on mutations of these other residues, which will be the subject of a separate report (Xiong, J., Farmer, C. S., Phillips, R. S., and Kurtz, D. M., Jr., manuscript in preparation). Finally, we note that, if preferred O_2 diffusional pathways through the protein matrix, such as parallel to the four-helix bundle axis (cf. Figure 2), exist in myoHr, then amino acid residues beyond the binding pocket could affect the association rate. Either site-directed or random mutagenesis could be used to address this possibility (*42, 43*).

ACKNOWLEDGMENT

We thank Ms. Kay Dennis for experimental assistance in cloning and overexpression of the Pg myoHr gene.

SUPPORTING INFORMATION AVAILABLE

Figure S1 showing the oligonucleotide sequence encoding the myoHr gene in pKD1-10 (1 page), description of the SOE mutagenesis protocol (2 pages), Table S1 of oligonucleotide sequences used in the SOE mutagenesis PCR reactions (1 page), Figures S2 and S3 showing far-UV CD and resonance Raman spectra of L104X myoHrs (2 pages), and Tables S2 and S3 of O_2 association/dissociation kinetic data at several temperatures and activation parameters (2 pages)(9 pages total). This material is available free of charge via the Internet at http://pubs.acs.org.

REFERENCES

1. Stenkamp, R. E. (1994) *Chem. Rev. 94*, 715−726.
2. Brunold, T. C., and Solomon, E. I. (1999) *J. Am. Chem. Soc. 121*, 8288−8295.
3. Lloyd, C. R., Eyring, E. M., and Ellis, W. R., Jr. (1995) *J. Am. Chem. Soc. 117*, 11993−11994.
4. Negri, A., Gedeschi, G., Bonomi, F., Zhang, J.-H., and Kurtz, D. M., Jr. (1994) *Biochim. Biophys. Acta 1208*, 277−285.
5. Sheriff, S., Hendrickson, W. A., and Smith, J. L. (1987) *J. Mol. Biol. 197*, 273−296.
6. Brunold, T. C., and Solomon, E. I. (1999) *J. Am. Chem. Soc. 121*, 8277−8287.
7. Feig, A. L., and Lippard, S. J. (1994) *Chem. Rev. 94*, 759−805.
8. Petrou, A. L., Armstrong, F. A., Sykes, A. G., Harrington, P. A., and Wilkins, R. G. (1981) *Biochim. Biophys. Acta 670*, 377−384.
9. Bates, G., Brunori, M., Amiconi, G., Antonini, E., and Wyman, J. (1968) *Biochemistry 7*, 3016−3020.
10. Lavalette, D., Tetreau, C., Brochon, J. C., and Livesey, A. (1991) *Eur. J. Biochem. 196*, 591−598.
11. Lavalette, D., and Tetreau, C. (1991) in *Structure and function of invertebrate oxygen carriers* (Vinogradov, S. N., and Kapp, O. H., Eds.) pp 191−198, Springer-Verlag, New York.
12. Yedgar, S., Tetreau, C., Gavish, B., and Lavalette, D. (1995) *Biophys. J. 68*, 665−670.
13. Sayle, R., and Milner-White, E. J. (1995) *Trends Biochem. Sci. 20*, 374−376.
14. Martins, L. J., Hill, C. P., and Ellis, W. R., Jr. (1997) *Biochemistry 36*, 7044−7049.
15. Raner, G. M., Martins, L. J., and Ellis, W. R., Jr. (1997) *Biochemistry 36*, 7037−7043.
16. Wilkins, P. C., and Wilkins, R. G. (1987) *Coord. Chem. Rev. 79*, 195−214.
17. Long, R. C., Zhang, J. H., Kurtz, D. M., Jr., Negri, A., Tedeschi, G., and Bonomi, F. (1992) *Biochim. Biophys. Acta 1122*, 136−142.
18. Sambrook, J., Fritsch, E. F., and Maniatis, T. (1990) *Molecular Cloning: A Laboratory Manual*, 2nd ed., Cold Spring Harbor Laboratory Press, Cold Spring Harbor, NY.

19. Ausubel, F. A., Brent, R., Kingston, R. E., Moore, D. D., Seidman, J. G., Smith, J. A., and Struhl, K. (1990) *Current Protocols in Molecular Biology*, Green Publishing and Wiley-Interscience, New York.
20. Schagger, H., and von Jagow, G. (1987) *Anal. Biochem. 166*, 368−379.
21. Hirel, P. H., Schmitter, M. J., Dessen, P., Fayat, G., and Blanquet, S. (1989) *Proc. Natl. Acad. Sci. U.S.A. 86*, 8247−8251.
22. Bau, R., Rees, D. C., Kurtz, D. M., Jr., Scott, R. A., Huang, H., Adams, M. W. W., and Eidsness, M. K. (1998) *J. Inorg. Biochem. 3*, 484−493.
23. Tabor, S. (1990) in *Current Protocols in Molecular Biology* (Ausubel, F. A., Brent, R., Kingston, R. E., Moore, D. D., Seidman, J. G., Smith, J. A., and Struhl, K., Eds.) pp 16.12.11−16.12.11, Green Publishing and Wiley-Interscience, New York.
24. Horton, R. M., Cai, Z. L., Ho, S. N., and Pease, L. R. (1990) *BioTechniques 8*, 528−535.
25. Studier, W. F., Rosenberg, A. H., Dunn, J. J., and Dubendorff, J. W. (1990) *Methods Enzymol. 185*, 60−89.
26. Johnson, B. H., and Hecht, M. H. (1994) *Bio/Technology 12*, 1357−1360.
27. Robitaille, P. M., and Kurtz, D. M. Jr. (1988) *Biochemistry 27*, 4458−4465.
28. Zhang, J. H., and Kurtz, D. M., Jr. (1992) *Proc. Natl. Acad. Sci. U.S.A. 89*, 7065−7069.
29. Klippenstein, G. L., Van Riper, D. A., and Oosterom, E. A. (1972) *J. Biol. Chem. 247*, 5959−5963.
30. Solomon, E. I., Tuczek, F., Root, D. E., and Brown, C. A. (1994) *Chem. Rev. 94*, 827−856.
31. Shiemke, A. K., Loehr, T. M., and Sanders-Loehr, J. (1984) *J. Am. Chem. Soc. 106*, 4951−4956.
32. Duff, L. L., Klippenstein, G. L., Shriver, D. F., and Klotz, I. M. (1981) *Proc. Natl. Acad. Sci. U.S.A. 78*, 4138−4140.
33. Shiemke, A. K., Loehr, T. M., and Sanders-Loehr, J. (1986) *J. Am. Chem. Soc. 108*, 2437−2443.
34. Que, L., Jr. (1988) in *Biological Applications of Raman Spectroscopy* (Spiro, T. G., Ed.) pp 491−521, Wiley, New York.
35. Michaud-Soret, I., Andersson, K. K., and Que, L., Jr. (1995) *Biochemistry 34*, 5504−5510.
36. Wilkins, R. G., and Harrington, P. C. (1983) *Adv. Inorg. Biochem. 5*, 51−85.
37. Armstrong, G. D., and Sykes, A. G. (1986) *Inorg. Chem. 25*, 3135−3139.
38. Feher, V. A., Baldwin, E. P., and Dahlquist, F. W. (1996) *Nat. Struct. Biol. 3*, 516−521.
39. Glickman, M. H., Cliff, S., Thiemens, M., and Klinman, J. P. (1997) *J. Am. Chem. Soc. 119*, 11357−11361.
40. Projahn, H.-D., Schindler, S., van Eldik, R., Fortier, D. G., Andrew, C. R., and Sykes, A. G. (1995) *Inorg. Chem. 34*, 5935−5941.
41. Farmer, C. S., Kurtz, D. M., Jr., Phillips, R. S., Ai, J., and Sanders-Loehr, J. (2000) *J. Biol. Chem.* (in press).
42. Olson, J. S., and Phillips, G. N., Jr. (1996) *J. Biol. Chem. 271*, 17596.
43. Huang, X., and Boxer, S. G. (1994) *Nat. Struct. Biol. 1*, 226−229.

BI9929397